J|A|C|S
ARTICLES
Published on Web 10/06/2006

Wetting Properties of Passivated Metal Nanocrystals at Liquid−Vapor Interfaces: A Computer Simulation Study

Kafui A. Tay and Fernando Bresme*

Contribution from the Department of Chemistry, Imperial College London, Exhibition Road, London SW7 2AZ, United Kingdom

Received March 20, 2006; E-mail: f.bresme@imperial.ac.uk

Abstract: Molecular dynamics simulations have been employed to determine the contact angles of alkylthiol passivated gold nanocrystals adsorbed at the air−water interface. Simulations were performed using butane-, dodecane-, and octadecanethiol passivated nanoparticles. We demonstrate how the length of the surfactant chain can profoundly influence the wetting behavior of these nanoparticles. All particles were found to be stable at the air−water interface, possessing large, well-defined contact angles. We find that the shape of the dodecane- and octadecanethiol particles is strongly perturbed by the interface. We also present an analysis of the orientational ordering of water molecules at the dodecane−water interface and around butane- and dodecanethiol passivated nanoparticles. The orientational ordering translates into an electrostatic field around the nanoparticles, the magnitude of which corresponds with that of the water liquid−vapor interface.

1. Introduction

For a metallic or semiconducting nanoparticle, its optical or electronic properties vary profoundly with its size.[1] Thus, the properties of a superlattice of nanoparticles can be tuned according to its constituent particles. More specifically, the possible manipulation of interparticle separations, particle size, and stoichiometry can produce macroscopic solids with tailored properties. To exploit such an approach it has been necessary to devise strategies for the construction of nanoparticulate arrays and lattices. One of the most straightforward approaches for constructing ordered superlattices is through particle dispersal at the air−water interface.[2,3] The success of such an approach relies upon a detailed understanding of the wetting behavior of the nanoparticles.

The current inability of experimental techniques to closely probe the wetting characteristics of nanoscale particles adsorbed at interfaces has meant that computational methods have been invaluable in elucidating the wetting behavior of these particles. Of particular importance is the applicability of macroscopic relations, such as Young's equation, in describing wetting phenomena at the nanoscale. Indeed, it has been demonstrated, with computer simulations of Lennard-Jones particles, that the wetting of nanometer-sized particles at liquid−vapor and liquid−liquid interfaces, can be reasonably described (down to roughly 1 nm) using Young's equation when either the fluid−fluid interfacial tensions are large or when the three-phase line has small curvature.[4−6] It has also been demonstrated that the stability of nonspherical particles at interfaces can have complex dependencies upon both the line tension and particle orientation.[7]

Langmuir trough techniques have long been considered an important experimental tool for obtaining information on the microstructure of monolayers dispersed at interfaces. It was previously thought that surface pressure−surface area isotherms could yield information on the contact angles of the dispersed particles. However, it has been demonstrated through computer simulations that the measured collapse pressure should be independent of the contact angle.[8,9] This suggests that such techniques have to be used with care in contact angle determination.

We consider here the wetting properties of gold nanocrystals passivated by alkylthiols. Nanoparticles have been extensively studied over recent years[10,11] with particular emphasis on passivated nanocrystals.[12,13] Computer simulations have been successfully employed to examine both the structure and thermodynamic characteristics of isolated particles,[14,15] and extensive experimental and computational work have determined the structural, thermal, and mechanical properties of their assemblies.[16−18] The phase behavior of nanoparticle dispersions has also been investigated with particular emphasis on understanding the complex structures formed at the air−water interface.[19−21]

(1) Daniel, M. C.; Astruc D. *Chem. Rev.* **2004**, *104*, 293−346.
(2) Fendler, J. H. *Curr. Opin. Colloid Interface Sci.* **1996**, *1*, 202−207.
(3) Fendler, J. H. *Chem. Mater.* **1996**, *8*, 1616−1624.
(4) Bresme, F.; Quirke, N. *Phys. Rev. Lett.* **1998**, *80*, 3791−3794.
(5) Bresme, F.; Quirke, N. *J. Chem. Phys.* **1999**, *110*, 3536−3547.
(6) Bresme, F.; Quirke, N. *Phys. Chem. Chem. Phys.* **1999**, *1*, 2149−2155.
(7) Faraudo, J.; Bresme, F. *J. Chem. Phys.* **2003**, *118*, 6518−6528.
(8) Fenwick N.; Bresme, F; Quirke, N. *J. Chem. Phys.* **2001**, *114*, 7274−7282.
(9) Powell, C.; Fenwick, N.; Bresme, F.; Quirke, N. *Colloids Surf., A* **2002**, *206*, 241−251.
(10) Cayre, O. J.; Paunov, V. N. *Langmuir* **2004**, *20*, 9594−9599.
(11) Shipway, A. N.; Katz, E.; Willner, I. *ChemPhysChem* **2000**, *1*, 18−52.
(12) Templeton, A. C.; Wuelfing, W. P.; Murray, R. W. *Acc. Chem. Res.* **2000**, *33*, 27−36.
(13) Rotello, V. M.; Shenar, R. *Acc. Chem. Res.* **2000**, *36*, 549−561.
(14) Luedtke, W. D.; Landman, U. *J. Phys. Chem.* **1996**, *100*, 13323−13329.
(15) Luedtke, W. D.; Landman, U. *J. Phys. Chem. B* **1998**, *102*, 6566−6572.
(16) Landman, U.; Luedtke, W. D. *Faraday Discuss.* **2003**, *125*, 1−22.
(17) Whetten, R. L.; Khoury, J. T.; Alvarez, M. M.; Murthy, S.; Vezmar, I.; Wang, Z. L.; Stephens, P. W.; Cleveland, C. L.; Luedtke, W. D.; Landman, U. *Adv. Mater.* **1996**, *8*, 428−433.
(18) Whetten, R. L.; Shafigullin, M. N.; Khoury, J. T.; Schaaff, T. G.; Vezmar, I.; Alvarez, M. M.; Wilkinson, A. *Acc. Chem. Res.* **1999**, *32*, 397−406.

10.1021/ja061901w CCC: $33.50

The hydrophobic nature of the alkylthiol passivating ligands ensures the stability of the nanoparticles at the air−water interface. Though the structure of water molecules at the oil−water interface is reasonably well understood through both computer simulations[22] and experiment,[23,24] the structure of water around hydrophobic solutes is less well so. It has been proposed that for small hydrophobes hydrogen bonding of water molecules persists around the particle. For larger particles the hydrogen bonding is depleted, bringing about a drying at the surface.[25,26] This drying can lead to strong attractions between extended hydrophobic surfaces. Thus, theories on the hydrophobic effect describe the phenomena as originating from structural changes in the hydration layer surrounding the hydrophobe.

Despite the relatively weak hydrogen bonding found between water molecules at extended hydrophobic surfaces, strong orientational ordering persists.[23] Similar ordering of water molecules has been observed for hydrophobic solutes in computer simulations.[27−29] Just as in the case of the liquid−vapor interface the ordering of interfacial molecules gives rise to a surface potential. The difficulty of experimental determination means that no value for the interfacial potentials across oil−water interfaces is available. Although this question has received much attention, there is little consensus on either the sign or the magnitude of the liquid−vapor interface potential.[30,31]

Previous simulation work has involved mainly structureless nanoparticles. This has enabled a systematic investigation of the influence of line tension, particulate size, particulate shape, and particle−solvent interaction strength on the wetting and drying transitions of ideal particulates. However, this simplification belies the fact that nanoparticles can possess complex structures which may influence their wetting behavior in unexpected ways. In addition to this, the solvent may itself possess its own "eccentricities", as is the case with water. Here we use a realistic model to determine the wetting behavior of alkanethiol passivated nanoparticles adsorbed at the air−water interface using molecular dynamics simulations. Specifically, we investigate the influence of chain length on the contact angle, particle shape, and particle orientation. To this end we perform simulations of nanoparticles adsorbed at interfaces for butane-, dodecane-, and octadecanethiol passivated nanoparticles. We also present an investigation of the orientational ordering of water molecules around solvated nanoparticles and examine the resulting surface potentials.

2. Methods

Molecular dynamics simulations have been used to investigate the wetting behavior of hydrophobic colloidal nanoparticles. In particular, we determine directly the equilibrium contact angles of butane-, dodecane-, and octadecanethiol passivated particles adsorbed at the air−water interface. We also investigate the orientational ordering of water molecules at both the planar dodecane−water interface and around butane- and dodecanethiol passivated nanoparticles in bulk water. All simulations were performed using the DLPOLY 2.0 molecular simulation package.[32] Unless stated otherwise all simulations were carried out at 298 K, within the canonical ensemble, and using the smooth particle mesh Ewald method (SPME).[33]

2.1. Molecular Model for the Passivated Nanoparticles. The crystalline core of gold atoms was modeled within a truncated octahedral motif consisting of a face-centered cubic lattice of 140 atoms as has been used in previous simulation studies.[9,14−16] Experimental findings have shown the existence of an energetically optimal sequence of gold nanocrystal structures, of which the Au_{140} nanocrystallite is a member.[17] Theoretical calculations determined that these structures are characterized by face-centered cubic lattices, generally possess truncated octahedral morphologies, and present good stability. We use the many-body Sutton−Chen potential parametrized for gold,[34,35]

$$U = \epsilon \sum_i \left[\frac{1}{2} \sum_{j \neq i} \left(\frac{a}{r_{ij}} \right)^n - C \sqrt{p_{ij}} \right] \quad p_{ij} = \sum_{j \neq i} \left(\frac{a}{r_{ij}} \right)^m \tag{1}$$

The parameters ϵ, a, and C are determined by equilibrium lattice parameters and lattice energies. The exponent pairs, n and m are fitted to elastic constants and r_{ij} is the distance between gold atoms i and j. For gold, $\epsilon = 9.383265$ kJ, $a = 4.080$ Å, $n = 10.0$, $m = 8.0$, and $C = 34.408$. The melting temperature predicted by this model for bulk gold is lower than the experimental one. Despite this, the Au_{140} cluster was found to be stable at 300 K.

The thiol−gold (SH−Au) interaction was approximated as a nonbonded $m-n$ potential. The parameters are compatible with the experimental findings of the thiol−gold bonding interaction.[36] The $m-n$ potential is defined as,[37]

$$U(r) = \frac{E_0}{n-m} \left[m \left(\frac{r_0}{r} \right)^n - n \left(\frac{r_0}{r} \right)^m \right] \tag{2}$$

where r is the distance between atoms, $E_0 = 38.6$ kJ mol^{-1}, $n = 8$, $m = 4$ and $r_0 = 2.9$ Å. It has been previously reported that the strength of the thiol−gold interaction can result in the penetration and hence disruption of the crystalline core by the sulfur pseudoatoms.[9] To counteract this the gold−gold interaction energy in the Sutton−Chen potential was increased by a factor of 5 to $\epsilon = 46.916325$ kJ. The sole effect of this change is to preserve the shape and lattice structure of the gold core during and after adsorption of the surfactants. The preserved morphology and crystallinity of nanocrystals after passivation is commonly observed with high-resolution electron microscopy.[17] The alkanethiol passivating chains were modeled using united atom potentials.[38] The alkanethiol intramolecular interactions were modeled using constraints for the bonds, harmonic potentials for angular degrees of freedom,

(19) Heath, J. R.; Knobler, C. M.; Leff, D. V. *J. Phys. Chem. B* **1997**, *101*, 189−197.
(20) Sear, R. P.; Chung, S.-W.; Markovich, G.; Gelbart, W. M.; Heath, J. R. *Phys. Rev. E* **1999**, *59*, R6255−R6258.
(21) Gelbart, W. M.; Sear, R. P.; Heath, J. R.; Chaney, S. *Faraday Discuss.* **1999**, *112*, 299−307.
(22) Jedlovsky, P.; Vincze, A.; Horvai, G. *Phys. Chem. Chem. Phys.* **2004**, *6*, 1874−1879.
(23) Scatena, L. F.; Brown, M. G.; Richmond, G. L. *Science* **2001**, *292*, 908−912.
(24) Brown, M. G.; Walker, D. S.; Raymond, E. A.; Richmond, G. L. *J. Phys. Chem. B.* **2003**, *107*, 237−244.
(25) Lum, K.; Chandler, D.; Weeks, J. D. *J. Phys. Chem. B* **1999**, *103*, 4570−4577.
(26) Chandler, D. *Nature* **2005**, *437*, 640−647.
(27) Huang, X.; Margulis, C. J.; Berne, B. J. *J. Phys. Chem. B* **2003**, *107*, 11742−11748.
(28) Mamatkulov, S. I.; Khabibullaev, P. K. *Langmuir* **2004**, *20*, 4756−4763.
(29) Raschke, T. M.; Levitt, M. *Proc. Natl. Acad. Sci. U.S.A.* **2005**, *102*, 6777−6782.
(30) Parfenyuk, V. I. *Colloid J.* **2002**, *64*, 588−595.
(31) Paluch, M. *Adv. Colloid Interface Sci.* **2002**, *84*, 27−45.
(32) Smith, W.; Forester, T. R. DLPOLY 2.0; CCLRC, Daresbury Laboratory, 1999.
(33) Essmann, U.; Perera, L.; Berkowitz, M. L.; Darden, T,; Lee, H.; Pedersen, L. G. *J. Chem. Phys.* **1995**, *103*, 8577−8593.
(34) Todd, B. D.; Lynden-Bell, R. M. *Surf. Sci.* **1995**, *328*, 170−170.
(35) Todd, B. D.; Lynden-Bell, R. M. *Surf. Sci.* **1993**, *281*, 191−206.
(36) Sellers, H.; Ulman, A.; Shnidman, Y.; Eilers, J. E. *J. Am. Chem. Soc.* **1993**, *115*, 9389−9401.
(37) Clarke, J. H. R.; Smith, W.; Woodcock, L. V. *J. Chem. Phys.* **1986**, *84*, 2290−2294.
(38) Ryckaert, J. P.; Bellemans, A. *Faraday Discuss.* **1978**, *66*, 95−106.

$$U_{\text{angle}}(\theta) = \frac{1}{2}k(\theta - \theta_0)^2 \quad (3)$$

and dihedral angle potentials for torsional interactions,

$$U_{\text{dihedral}}(\phi) = \frac{1}{2}a_1(1 + \cos(\phi)) + \frac{1}{2}a_2(1 - \cos(2\phi)) + \frac{1}{2}a_3(1 + \cos(3\phi)) \quad (4)$$

The parameters found in eqs 3 and 4, are listed in Table 1. Standard nonbonded interactions were modeled with Lennard-Jones 12−6 potentials[39] and were employed with a cutoff of 12 Å. These parameters are found in Table 2.

2.2. Preparation of the Passivated Au_{140} Nanoparticles. The Au_{140} passivated nanoparticle was prepared using a method similar to that employed by Luedtke and Landman.[15] The Au_{140} nanocrystal was allowed to equilibrate within a solution of butanethiol molecules for 1 ns (500×10^3 time steps) at 200 K. The temperature was then raised to 500 K in steps of 50 K (20×10^3 time steps each, 20 ps). This allowed for the desorption of excess butanethiols from the cluster surface and the diffusion of surfactant molecules around adsorption sites. In this way a compact monolayer of 62 surfactant molecules on the surface of the cluster was generated. The adsorbed thiols formed a hexagonal close packed structure in agreement with the work of Luedtke and Landman. Surfactants found not to be adsorbed were removed and the remaining nanocrystal and surfactants further equilibrated. The dodecanethiol and octadecanethiol passivated nanoparticles were generated by extension of the surfactant chains. To avoid the trapping of surfactants in nonequilibrium conformations the new structures were then simulated at 500 K for 100 ps (50×10^3 time steps) before being slowly relaxed to 300 K in steps of 50 K (50×10^3 time steps).

Typically, the surface density per surfactant molecule on planar gold surfaces is 21.4 Å^2 and 20.6 Å^2 on Au(111) and Au(100), respectively.[14] Geometric arguments have been employed to suggest that the sulfur packing density on nanocrystallites is approximately 50% higher than on analogous planar surfaces.[40] For our particles the mean distance between sulfur atoms and the center of the crystalline core is 9.12 Å. If we imagine our 62 surfactants to be adsorbed onto a sphere (of radius 9.12 Å), we have a surfactant density of 16.9 Å^2 per molecule. It has been reported that the alkanethiolate surface density on nanoparticles is 15.4 Å^2 per molecule.[41] If we approximate the crystalline core as an octahedron with edge lengths (l) of 16 Å, the surface density is approximately 14.3 Å^2 per molecule (where the surface area is given by $2l^2\sqrt{3}$).

2.3. Nanoparticle Adsorption at the Air−Water Interface. The butanethiol passivated nanoparticle was placed just above a slab of 2619 water molecules (with cross sectional area 56 Å × 56 Å, see Figure 1). The lateral dimensions of the water slab were chosen to avoid interactions between the nanoparticle and its periodic image and also to ensure the existence of "bulk" water around the particle far from the nanoparticle−water interface. The thickness of the water slab was approximately 25 Å. The particle was allowed to adsorb onto the surface of the water slab and equilibrate over a simulation time of 4 ns (2×10^6 steps). The water molecules were modeled using the extended simple point charge model.[42] The water−gold interaction energy was modeled as a 12-6 Lennard-Jones potential with parameters fitted to reproduce adsorption energies comparable to experiments.[43] The Au−O interaction energy, ϵ, was 8.28 kJ/mol. The collision diameter, σ, was obtained through the Lorentz−Berthelot combining rules. No interaction between the water hydrogens and gold atoms was included. Simulations were also performed using the dodecane- and octadecanethiol passivated nanoparticles. Due to the computational expense of these simulations the total simulation time was reduced to 3 ns for the dodecanethiol particle and 1.5 ns for the octadecanethiol particle. In both cases larger slabs of water were used incorporating 3798 and 4728 water molecules respectively, with interfacial areas increased to 68 Å × 68 Å and 75 Å × 75 Å. To construct a density profile atom positions were recorded every picosecond (500 steps). By approximating the particle as a sphere we can calculate the contact angle, θ, of the particle at the interface with the following equation,

$$\cos\theta = \frac{h}{r} - 1 \quad (5)$$

where r is the radius of the particle, and h is the average depth of

Table 1. Surfactant Intermolecular Interactions[9]

interacting groups	parameters[a]
rigid bond CH_3-CH_2	1.54
rigid bond CH_2-CH_2	1.54
rigid bond CH_2-SH	1.82
harmonic angle $CH_2-CH_2-CH_3$	$k = 519.73$
	$\theta_0 = 114.4$
harmonic angle CH_2-CH_2-SH	$k = 519.73$
	$\theta_0 = 114.4$
dihedral angle $CH_2-CH_2-CH_2-SH$	$a_1 = 5.9046$
	$a_2 = -1.134$
	$a_3 = 13.1608$
dihedral angle $CH_2-CH_2-CH_2-CH_x$	$a_1 = 5.9046$
	$a_2 = -1.134$
	$a_3 = 13.1608$

[a] Distance terms in Å, angles in degrees and energy in kJ/mol.

Table 2. Lennard-Jones Parameters for Standard Nonbonded Interactions[9]

	ϵ (kJ/mol)	σ (Å)
CH_3	0.9478	3.930
CH_2	0.3908	3.930
SH	1.6629	4.450
Au	3.2288	2.737

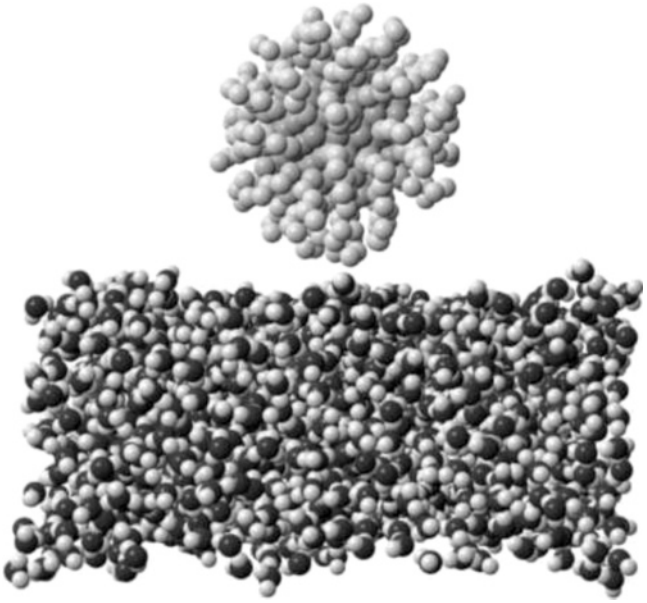

Figure 1. Snapshot of a molecular dynamics simulation. A butanethiol passivated nanocrystal is allowed to slowly adsorb onto a slab of 2691 water molecules at 298 K.

(39) Xia, T. K.; Ouyang, J.; Ribarsky, M. W.; Landman, U. *Phys. Rev. Lett.* **1992**, *69*, 1967−1970.
(40) Leff, D. V.; Ohara, P. C.; Heath, J. R.; Gelbart, W. M. *J. Phys. Chem.* **1995**, *99*, 7036−7041.
(41) Pradeep, T.; Sandhyarani, N. *Pure Appl. Chem.* **2002**, *74*, 1593−1607.
(42) Berendsen, H. J. C.; Grigera, J. R.; Straatsma, T. P. *J. Phys. Chem.* **1987**, *91*, 6269−6271.
(43) Lee, S.; Staehle, R. W. *Z. Metallkd.* **1997**, *88*, 880−886.

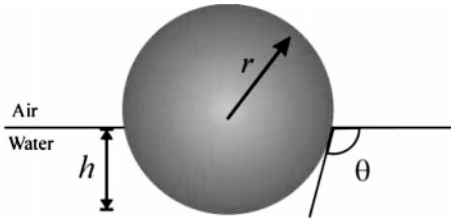

Figure 2. Schematic illustrating the contact angle of a spherical particle, with radius *r*, adsorbed at the air−water interface.

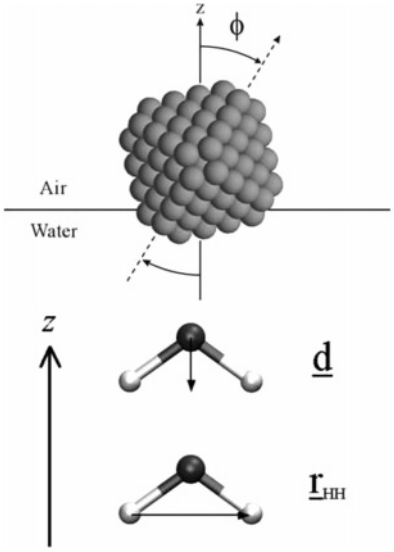

Figure 3. (Top) Orientation of the crystalline core of the nanoparticles is measured with respect to the *z*-axis. A vector is assigned to the crystal passing through its center between opposing vertexes. The tilt-angle, ϕ, is defined as the angle between the *z*-axis vector and this crystal axis vector. We take into account the rotational symmetry of the Au_{140} crystal and thus the value of ϕ varies between 0 and 90°. (Bottom) Orientation of water molecules is described by two vectors: the molecular dipole moment vector, **d**, and $\mathbf{r}_{HH}$, the vector joining the two hydrogen atoms. The *z*-axis vector is normal to the interface.

immersion of the particle into the interface (see Figure 2). We also monitor the orientation of the nanocrystal with respect to the *z*-axis throughout the simulation. A vector is defined passing through the center of the Au_{140} crystal between two opposing vertexes (Figure 3). The tilt-angle, ϕ, is the angle between the *z*-axis vector and this crystal axis vector. We take into account the rotational symmetry of the Au_{140} crystal, and thus the value of ϕ varies between 0 and 90°.

2.4. Planar Dodecane−Water Interface. To better understand the nature of the hydrophobic nanoparticle−water interface we performed simulations on a planar oil−water interface using dodecane. A lattice of 186 dodecane molecules was allowed to condense and equilibrate in an elongated simulation box ($L_x = L_y = 40$ Å, and $L_z = 200$ Å). To ensure that the chains were not trapped in nonequilibrium conformations the system was heated to 425 K and cooled to 300 K in 25 K steps. To create the alkane−water interface 2180 water molecules were then added to the simulation box on one side of the alkane slab. This system was then allowed to equilibrate for 100 ps (50 000 steps). The positions of the atoms were then translated to center the interface about $z = 0$, with the water phase on the positive side of the *z*-axis. The system was then run at 298 K for 1 ns (500 000 steps). The density profile along the *z*-axis was calculated using configurations from each time step of the simulation. The electrostatic field, *E*, is computed using the Gauss theorem,

$$E(z) = \frac{1}{\epsilon_0}\int_{-x}^{z} \rho(z')\,dz' \qquad (6)$$

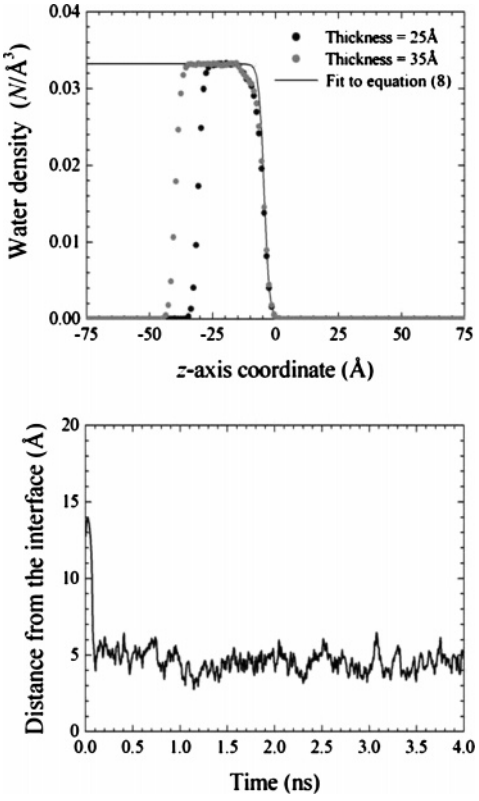

Figure 4. (Top) *z*-axis density profiles of the water molecules in the simulation of a butanethiol passivated nanoparticle adsorbed at the air−water interface. (Bottom) Distance between center of the butaenthiol passivated nanoparticle and the air−water interface throughout the simulation.

where $\rho(z)$ is the charge density and ϵ_0 is the vacuum permittivity. The electrostatic potential, ϕ, is computed by integration of the field,

$$\phi(z) = -\int_{-\infty}^{z} E(z')\,dz' \qquad (7)$$

The orientation of the water molecules was recorded with respect to two molecular vectors. In a fashion similar to recent work[22] we determine **d**, the dipole vector of each water molecule and $\mathbf{r}_{HH}$, the vector joining the two hydrogen atoms (see Figure 3). The orientation of the molecules is characterized by the angles α and β formed between the vectors (**d** and $\mathbf{r}_{HH}$) and the *z*-axis.

2.5. Passivated Nanoparticles in Bulk Water. We consider here butane- and dodecanethiol passivated nanoparticles in bulk water. These systems were simulated to investigate the orientational and electrostatic properties of the water−nanoparticle interface. We contrast the water structure and electrostatic characteristics with the dodecane−water interface. For ease of computation we forego cuboidal boundary conditions and use a simulation cell with truncated octahedral symmetry. The face-to-face distance of the cell, *d*, was approximately 65 Å (the simulation cell contained 4443 water molecules). The more spherical shape of the cell facilitates the simulation of a particle in solution by reducing the number of solvent molecules necessary to create the bulk. The nanoparticle is centered in the middle of the simulation cell, and the gold atoms are "frozen" while all other atoms are free to move. The system is simulated for a total time of 1 ns (500×10^3 time steps with 5×10^4 equilibration) under the NPT ensemble at zero pressure. At every step after equilibration a radial density profile is calculated from the center of the nanoparticle. As with the planar interface we measure the electrostatic field using an equation similar to eq 6 adapted to the spherical symmetry of the nanoparticle, and the orientation of the water molecules in terms of the two molecular vectors **d** and $\mathbf{r}_{HH}$. The angles α and β are measured with respect to another vector from

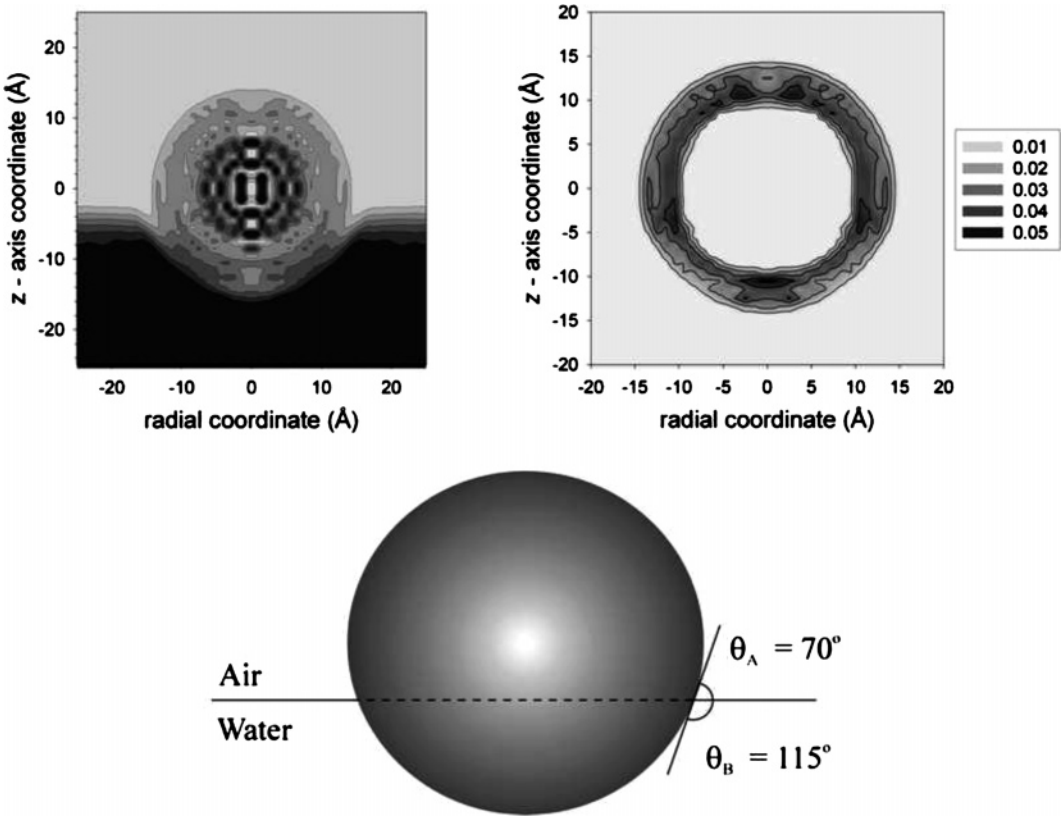

Figure 5. (Top left) All-atom density profile of the butanethiol passivated nanoparticle adsorbed at the air−water interface. (Top right) Carbon pseudoatom density profile of the particle at the interface (units of the plot are N Å^{-3}, number of pseudoatoms per ångström cubed). (Bottom) Schematic depicting the supra- and subsurface contact angles. The error in the contact angles is ±2°.

the water molecule to the center of the simulation cell (and hence normal to the particle−water interface). This procedure was repeated for a dodecanethiol passivated nanoparticle, for which the face-to-face distance of the cell was close to 70 Å (the simulation cell contained 4760 water molecules).

3. Results and Discussion

3.1. Nanoparticles Adsorbed at Interfaces. Figure 4 shows the *z*-axis density profile of the water molecules in the simulation cell containing the butanethiol passivated nanoparticle. The density profile was obtained from the final 0.5 ns of the simulation. To determine the dependency of the contact angle on the thickness of the water slab we have performed an additional simulation. In this case the thickness of the water slab was extended to 35 Å and the system simulated for a further nanosecond. The perturbation in the density profiles is due to the presence of the adsorbed particle at the interface. We estimated the position of the Gibbs dividing surface by fitting the density profile of the water molecules to the following equation,[44]

$$\rho(z) = \frac{1}{2}(\rho_l + \rho_v) - \frac{1}{2}(\rho_l - \rho_v)\tanh\left[\frac{(z - z_e)}{w}\right] \qquad (8)$$

where ρ_v and ρ_l represent the vapor and liquid coexistence densities, z_e represents the location of the equimolar dividing surface, and w is a measure of the thickness of the interface. We use the equimolar dividing surface to determine the position of the nanoparticle relative to the interface. The center of the nanoparticle is located at $z = 0$ Å. In both cases the interface is located at the same position.

At the start of the simulation the nanoparticle slowly adsorbs on to the interface. By examination of the position of the particle above the interface it can be seen that by 1 ns the particle has equilibrated at the interface (Figure 4). Figure 5 shows an all-atom cylindrical density profile of the butanethiol passivated nanoparticle adsorbed at the interface. Also shown is the surfactant pseudoatom density profile. The density is plotted in terms of N/Å^3(number of pseudoatoms Å^{-3}). Both profiles are computed using atom configurations from the final 0.5 ns of the simulation. The center of the nanoparticle core is taken as the origin, and the profile is computed in terms of the *z*-axis coordinate and the cylindrical radial coordinate, *r*. The density at a given point (*z*,*r*) is averaged over all azimuthal angles. The slight perturbation in the shape of the particle near the position of the interface highlights its softness. This softness appears to be characteristic of such passivated nanoparticles and has been previously observed in computer simulations of dodecanethiol passivated nanoparticles in a vacuum.[45] To best describe the shape of the particle we determine both a supra- and subsurface contact angle. The result is shown in Figure 5. We extract from the interpolated carbon pseudoatom density profile, all points (*z*,*r*) with density $0.01 \pm 1.0 \times 10^{-3}$ pseudoatoms Å^{-3}. The extracted data provides contours describing the inner and outer shape of the nanoparticle (Figure 6). The outer profile is reduced to a composite of circles from which we can estimate the contact angles. For the butanethiol passivated nanoparticle we fit two circles to the subsurface shape of the particle and another two

(44) Rowlinson, J. S.; Widom, B. *Molecular Theory of Capillarity*; Oxford Science, New York, 1989.

(45) Tay, K. A.; Bresme, F. *Mol. Simul.* **2005**, *31*, 515−526.

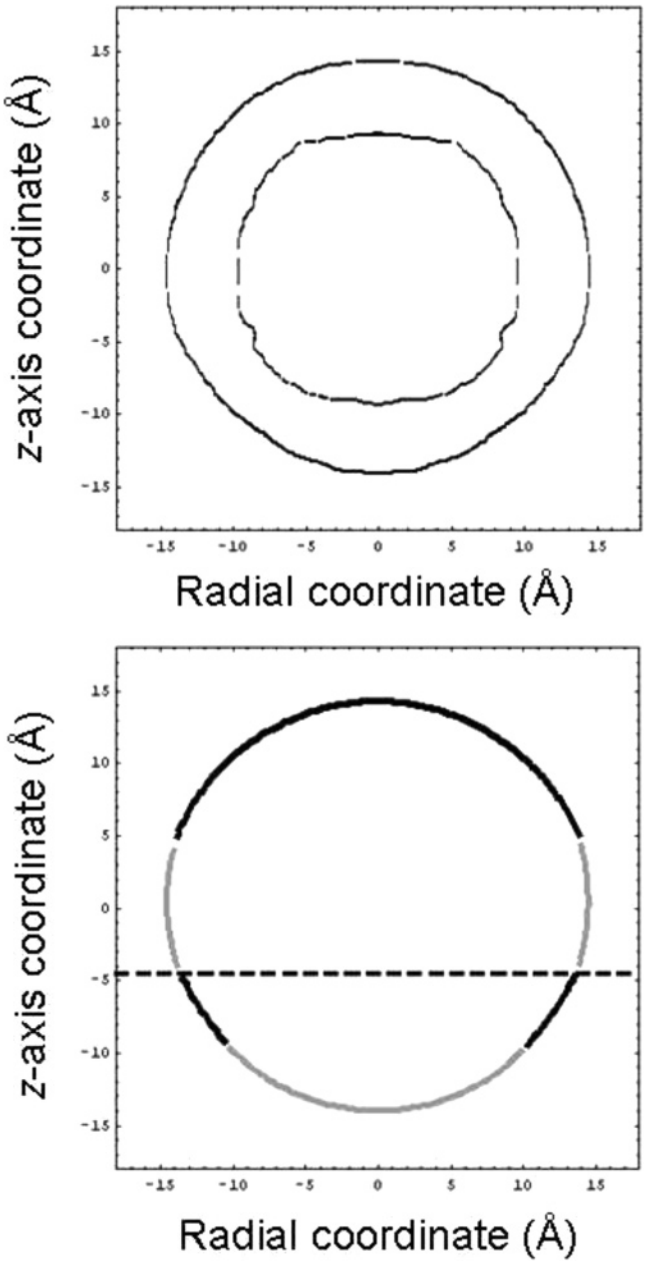

Figure 6. (Top) Contour profile for the butanethiol passivated nanoparticle at the interface. (Bottom) Outer profile of the nanoparticle is fitted to the three circles. The dashed line represents the position of the interface.

to the suprasurface. The choice of density is not physical but must provide an appropriate description of the outer profile of all the particles considered. The same criteria is applied in the analysis of all three particles. By considering the radius of the circles (r) and the distance between the center of the circles and the interface ($r - h$), the contact angles can be computed from eq 5. For the butanethiol passivated nanoparticle the subsurface contact angle is 115° and the suprasurface angle is 70°. To check for sufficient equilibration the contact angles are calculated again using data from the penultimate 0.5 ns of the simulation. The results are found to be consistent. The stability of the particle at the interface and the size of the subsurface angle confirm the particle's hydrophobicity. The thickness of the interface was not found to influence the contact angles of the adsorbed particle. The error in the contact angles is ±2° and is computed from the standard deviation associated with

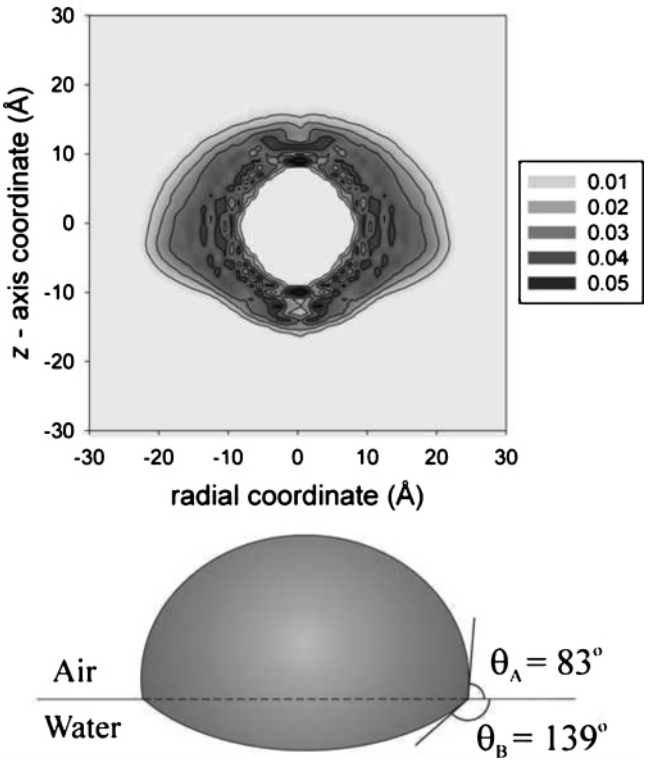

Figure 7. (Top) Carbon pseudoatom density profile of the dodecanethiol passivated particle at the interface (units of the plot are N Å^{-3}, number of pseudoatoms per ångström cubed). (Bottom) Schematic depicting the supra- and subsurface contact angles. The error in contact angles is ±2°.

the mean position of the interface. The density profiles and contact angles of the dodecanethiol and octadecanethiol particles were obtained in a similar fashion (Figures 7 and 8). In both cases the structure of the particles is significantly perturbed by the interface. The subsurface contact angles are equally large at around 140°, whereas the suprasurface contact angle is larger for the octadecanethiol particle. The errors in the contact angles of the dodecanethiol and octadecanethiol passivated nanoparticles are ±2° and ±1°, respectively.

For a particle adsorbed at the air−water interface the contact angle increases with increasing particle hydrophobicity as the particle sits higher up at the interface minimizing the free energy of the system. It may be expected that particles with longer-chain surfactants are more hydrophobic due to the larger particle−liquid interfacial tension. This is borne out by the fact that the longer-chain particles (C_{12} and C_{18}) show considerably larger contact angles than the shorter-chain particles. However, we also see a shift in the shape of the nanoparticle from particulate to something more akin to a liquid lens. This ability of the particle to deform can be linked to the ratio of the surfactant chain length to the core radius. This measure of "softness" has been used successfully, in both computer simulations and experiment, to rationalize the crystal structures of nanoparticle superlattices.[16,18] Nanoparticles for which the chain length is comparable to, or longer than, the radius of the crystalline core can be expected to exhibit a degree of softness. This manifests itself in a large perturbation of the particle shape at the interface. For a perfectly spherical particle the sum of the supra- and subsurface contact angles is 180°. The deviation from this value can be taken as the degree of perturbation undergone by the particle at the interface. For our simulations

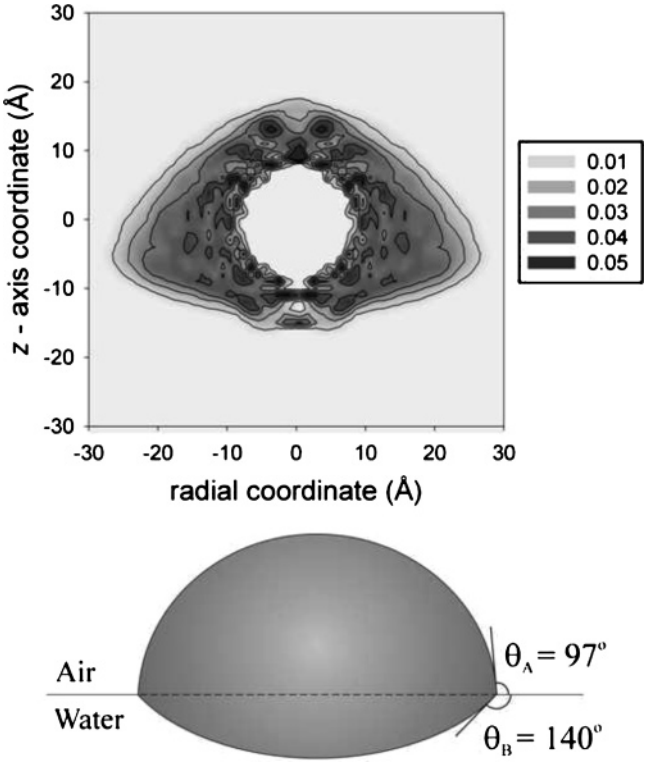

Figure 8. (Top) Carbon pseudoatom density profile of the octadecanethiol passivated particle at the interface (units of the plot are N Å^{-3}, number of pseudoatoms per ångström cubed). (Bottom) Schematic depicting the supra- and subsurface contact angles. The error in the contact angles in ±1°.

the deviation increases with increasing chain length from 5°-(C_4), to 42°(C_{12}), to 57°(C_{18}). In a vacuum the surfactant chains are not fully extended from the crystal surface but do exist in a predominantly trans state.[45] At the interface "spreading" of the larger particles is facilitated by extension of the chains located within the interfacial region. The final shape of the particle arises from a combination of the interfacial tensions, the line tension, and the conformational restrictions of the tethered surfactant chains. It may be argued that the line tension has little influence in these systems as the large surface tension of the air−water interface suggests that a very large line tension is necessary to significantly change the contact angles.[6]

The large increase in the subsurface contact angle from the butanethiol to the dodecanethiol particle can be understood in terms of the large increase in hydrophobicity. However, a further increase in the chain length appears to have no effect on the subsurface contact angle. This is reminiscent of the behavior of water droplets on self-assembled monolayers (SAMs) of alkanethiolates on planar gold surfaces.[46] In such cases the advancing contact angles of the water droplets were found to be consistently within the range 111−114° for C_n (n being the number of carbon atoms) greater than 10. For shorter-chain lengths the contact angles were progressively lower. Results from simulation work on similar planar systems show slightly higher contact angles than these. Hautman and Klein obtained a contact angle of 135° ± 15° for a microscopic water droplet on a dodecanethiol covered surface at 300 K.[47] Using similar methods Srivastava et al. simulated water droplets on pentade-

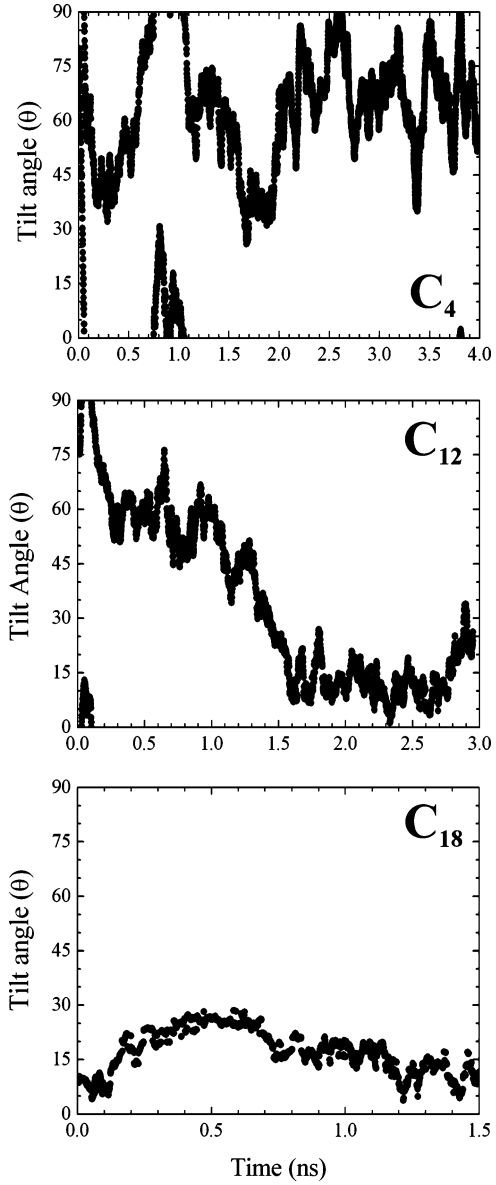

Figure 9. Variation of the tilt-angle, θ, with time for all three nanoparticles at the interface.

cane- and hexadecanethiol SAMs, yielding contact angles of 129° ± 1 and 128° ± 1, respectively. Comparisons are often made between SAMs on planar (2D) and particulate (3D) surfaces. Certainly, it has been argued that 3D SAMs are representative of 2D SAMs and, as thus, are important in generating further insight into the structure and dynamics of these systems.[48] However, it is important to note that both computer simulations and experiments reveal that the packing densities of surfactant chains on particulate surfaces are significantly higher than their planar equivalents.[15,41] This may produce significantly different wetting characteristics. Figure 9 shows the tilt angles of the crystal cores for each of the nanoparticles throughout the simulations. While the time-averaged particle shape at the interface can be resolved within the simulation time, it is clear that the dynamics of the crystalline core is far slower. The butanethiol passivated particle appears to be converging toward a tilt angle within the range 50−70°.

(46) Bain, C. D.; Troughton, E. B.; Tao, Y.; Evall, J.; Whitesides, G. M.; Nuzzo, R. G. *J. Am. Chem. Soc.* **1989**, *111*, 321−335.
(47) Hautman, J.; Klein, M. L. *Phys. Rev. Lett.* **1991**, *67*, 1763−1766.
(48) Badia, A.; Lennox, R. B. *Acc. Chem. Res.* **2000**, *33*, 475−481.

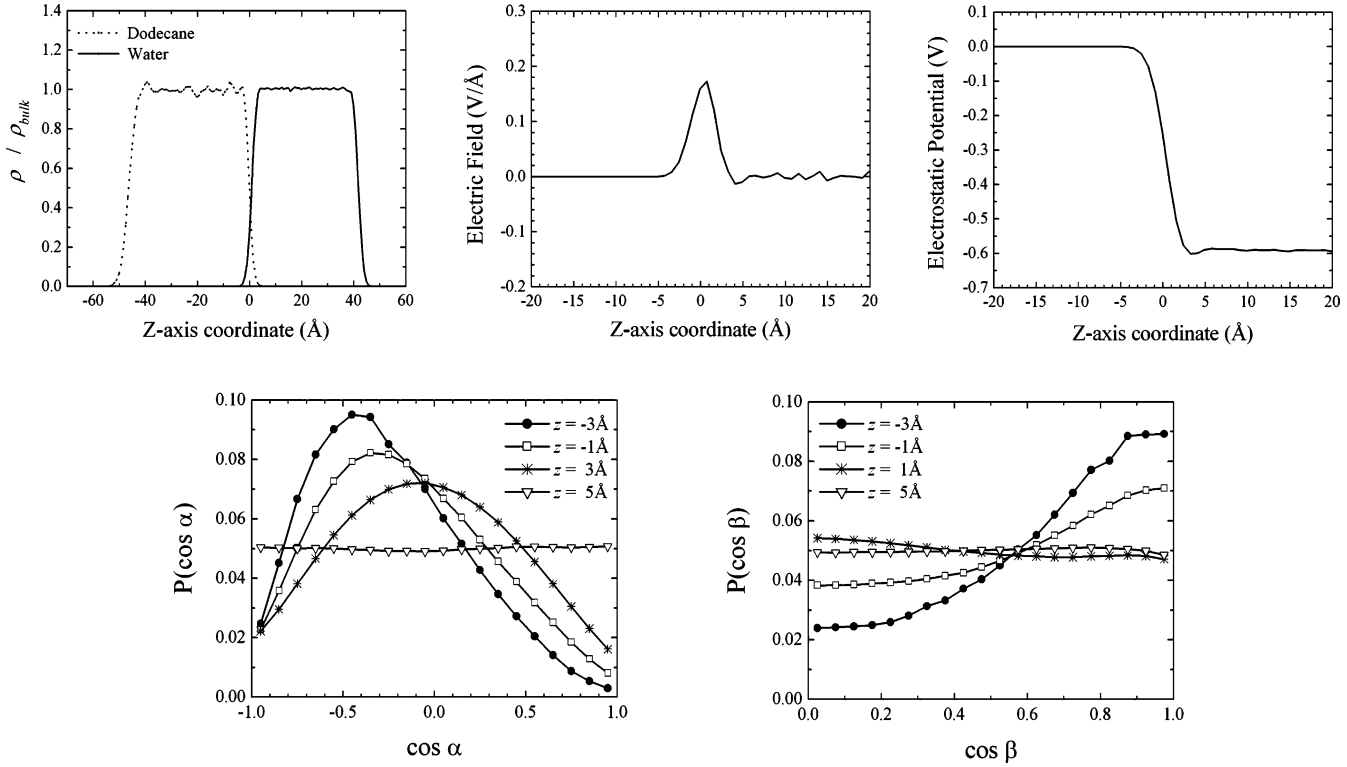

Figure 10. (Top) Density, electric field, and electrostatic potential profiles across a dodecane−water interface. (Bottom) Orientational distributions for the water molecules in terms of the angles α and β.

At this angle the crystal axis vector cuts diagonally through the *xy*-plane (the plane of the interface). In this configuration the nanocrystal sits on one of its edges with the two adjoining (111) facets facing the interface. That the nanoparticle appears to exhibit a preferred orientation at ambient temperatures suggests quite a clear nondegeneracy with regard to the different orientational configurations. We suggest that this preferred orientation is a result of the nanocrystal geometry and, as such, would appear for any set of potentials which reproduces the intrinsic hydrophobicity of the nanoparticles. In the case of the larger particles the simulation time is insufficient to elucidate any preferred orientation. The larger particles having both a larger mass and greater adsorption energy exhibit slower dynamics. This is clearly seen when contrasting the three graphs. The change in nanocrystal orientation over time is slowest for the octadecanethiol passivated particle. It should be emphasized that the existence of preferred orientations is most likely to be more significant for smaller nanocrystals, such as those studied here, where edges and apexes occupy a significant proportion of the surface.

3.2. Orientational Ordering of Water Molecules and Electrostatic Potentials. The *z*-axis density profile displayed in Figure 10 is typical of planar oil−water interfaces and is in agreement with earlier work.[49] Bulk densities agree with experimental values. The interface is centered around $z = 0$ Å with the water phase on the positive side of the *xy*-plane. The limited overlap of density profiles highlights the immiscibility of the two liquids. The water molecule profile at the interface is monotonic with no visible atomic layering and in this respect is similar to profiles obtained for the liquid−vapor water interface using the same model.[50] The electric field and electrostatic profiles shown here are also very close to results obtained for the liquid−vapor interface. We report here an electrostatic surface potential of −0.59 V. This result is higher than the figure of −0.5 V determined by Mamatkulov et al. for water (SPC/E) close to a planar hydrophobic wall[28] and the −0.546 V obtained for the liquid−vapor interface.[50]

The bottom graphs in Figure 10 detail the distributions of the two angles α and β. It is clear that strong orientation of the water molecules occurs on the dodecane side of the interface. For water molecules in this region (at $z = -1$ Å and −3 Å) the angle between the molecular dipole and the *z*-axis is generally greater than 90°, pointing toward the oil phase. On the water side of the interface ($z = 3$ Å) the dipole sits parallel to the interface. By $z = 5$ Å no preferred orientation of the molecular dipole exists. The distribution of the β angle also shows a preferred orientation on the dodecane side of the interface with values close to and at 0°. On the water side of the interface the β angle distribution peaks at 90°. The weak preference for this orientation, where the plane of the molecule lies parallel to the interface, disappears quickly on descending further into the bulk. Thus, for the water molecules on the oil side of the interface the plane of the molecule is predominantly perpendicular to the interface with one of its O−H bonds pointing toward the oil phase. At the interface the plane of the molecules tends to be parallel with the interface. This orientational distribution is in strong agreement with recent simulation work[22] and complements the experimental picture of these interfaces.[23]

The density profile for the butanethiol passivated nanoparticle is markedly different from the planar dodecane−water interface (Figure 11). Here we see that the oxygen and hydrogen density

(49) Pohorille, A.; Wilson, M. A. *J. Mol. Struct. (THEOCHEM)* **1993**, *284*, 271−298.

(50) Sokhan, V. P.; Tildesley, D. J. *Mol. Phys.* **1997**, *92*, 625−640.

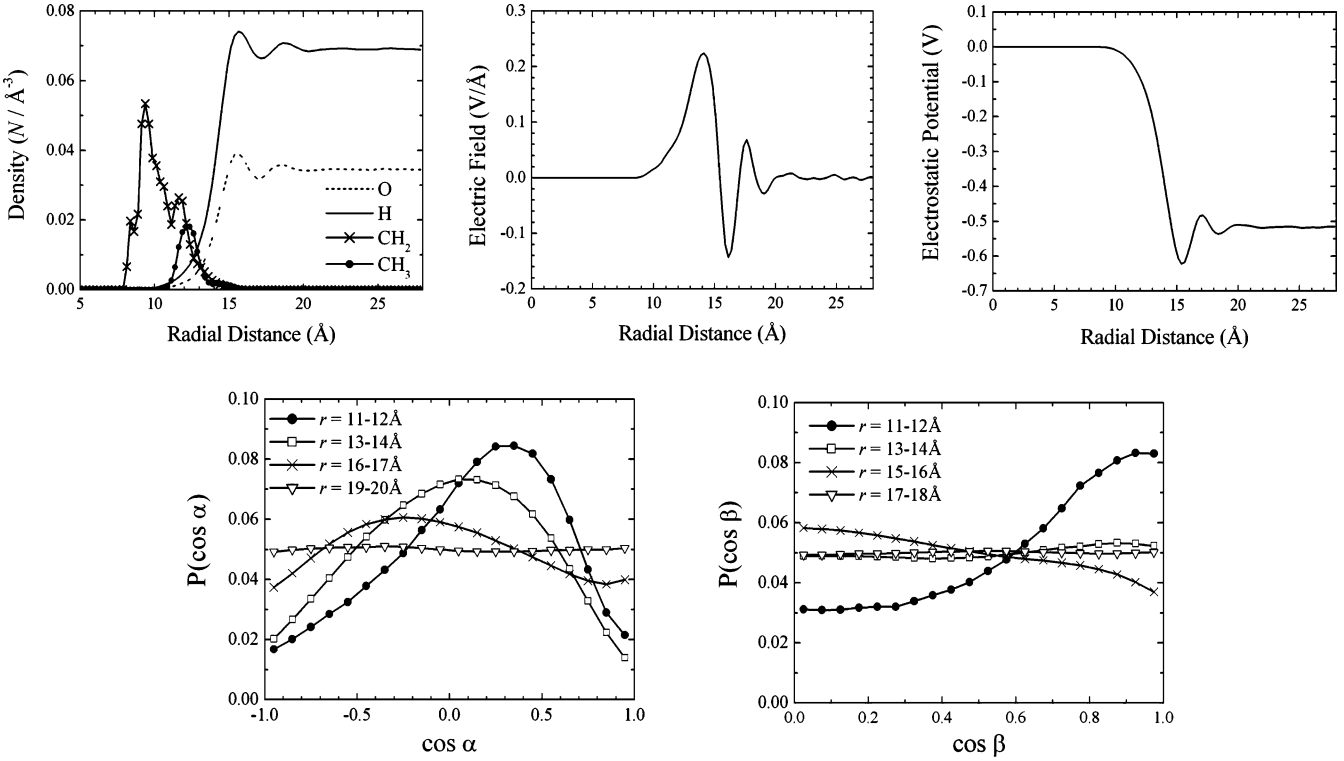

Figure 11. (Top) Radial density, electric field, and electrostatic potential profiles of a butanethiol passivated particle in bulk water. (Bottom,) Orientational distributions for the water molecules.

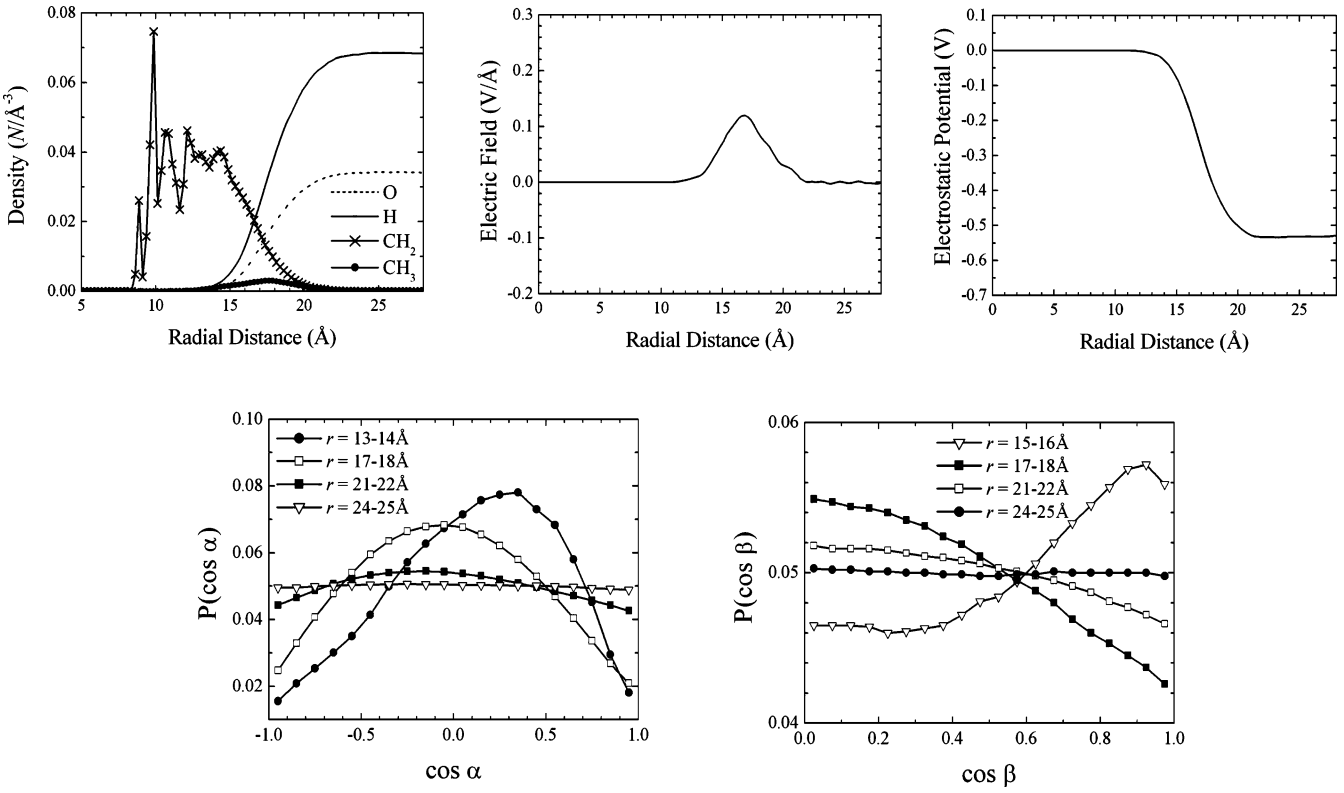

Figure 12. (Top) Radial density, electric field, and electrostatic potential profiles of a dodecanethiol passivated particle in bulk water. (Bottom) Orientational distributions for the water molecules.

profiles are not monotonic but exhibit oscillations typical of atomic layering. This structuring of the water molecules suggests the existence of a hydrogen-bonded network around the nanoparticle. This result compares favorably with the work of Mamatkulov et al.[28] in which they simulate spherical nonpolar solutes with radii in the range 4−10 Å in bulk water. The atomic layering is reflected in the significant oscillations found within the electric field and the electrostatic potential. In this case the electrostatic potential is −0.52 V, of the same magnitude as the dodecane−water interface and the liquid−vapor interface

of water (SPC/E model). The distributions of the angles α and β show the same trends as that of the planar interface.

The oxygen and hydrogen density profiles for the dodecanethiol passivated nanoparticle are monotonic, resembling the planar interface. This shows how the water structure around a small hydrophobe can resemble that of an extended surface. The result is comparable to recent work exploring the molecular structure of an oil−water interface where the alkyl chains are tethered to a planar support.[51] The potential profile is smoother but of comparable magnitude to the previous cases at −0.53V. The α and β angle distributions show similar orientational ordering to that found in both the planar and butanethiol systems. The respective radii of the butanethiol and dodecanethiol passivated nanoparticles are approximately 15 Å and 21 Å. That the time-averaged structure of water molecules around the particles can change so dramatically upon an increase in size is a clear indication of the significance of hydrophobe curvature.

4. Conclusion

We have investigated the wetting behavior of gold nanocrystals passivated with short- and long-chain alkylthiols (from butane- to octadecanethiol). The nanoparticles studied here are typical of those investigated in experiments.[19,40] We have been able to determine directly the contact angles of these particles. The particles are all stable at the interface with large contact angles. Clearly, the length of the passivating chain has a profound influence on the wetting behavior of these particles. The nanocrystals passivated with longer surfactant chains exhibit larger contact angles and significant shape deformation at the air−water interface. The degree of perturbation in the shape of the particles increases with chain length. Thus, the notion of these particles as relatively hard hydrophobic spheres is incorrect, but rather they appear to exist somewhere between particles and liquid lenses. It should be noted that this result is specifically applicable to the case when the length of the surfactant chain is comparable to, or larger than, the radius of the crystalline core. It is expected that much larger nanocrystals passivated with similar surfactants will also exhibit large contact angles, but with little or no shape deformation. Thus, we emphasize that a correct understanding of the wetting behavior of alkylthiol passivated nanocrystals can only be obtained by consideration of the relative dimensions of both the crystalline core and the passivating agent. Indeed, this notion has been successfully utilized to rationalize the crystal structures of superlattices formed of these particles.[16,18] The dynamics of the crystalline core are such that longer time scales, on the order of at least several nanoseconds, are needed to confirm the existence of preferred orientations. Interestingly our simulations suggest that the butanethiol passivated nanocrystal exhibits a preferred orientation at the interface. This result can be of relevance to molecular electronics, where nanocrystal orientation in superlattices can influence electron tunneling processes. We have also shown that orientational ordering of water molecules exists around these particles just as it does for the case of the planar interface. Indeed, the simulations presented here represent the range of possibilities for hydrophobes in water (small hydrophobes, larger hydrophobes, and the limit of the planar interface). The ordering at the interface of these particles brings about a surface potential comparable in magnitude to that of the planar interface. This is despite differences in the structure of water at these interfaces. Our results therefore support the existence of a significant electrostatic potential in the nanoparticle−water subphase.

Acknowledgment. We thank the EPSRC for funding. Computer resources on HPCx were provided via the UK's HPC Materials Chemistry Consortium (EPSRC grant EP/D504872). We would like to acknowledge the Barcelona Supercomputer Center (Spain) for providing resources on the *Mare Nostrum* Supercomputer, and the London eScience at Imperial College London (UK) for resources in the Viking cluster.

JA061901W

(51) Ashbaugh, H. S.; Pratt, L. R.; Paulaitis, M. E.; Clohecy, J.; Beck, T. L. *J. Am. Chem. Soc.* **2005**, *127*, 2808−2809.